Green, K., Champneys, AR., Friswell, MI., & Munoz, AM. (2008). Investigation of a multi-ball, automatic dynamic balancing mechanisms for eccentric rotors. *Philosophical Transactions of the Royal Society A: Mathematical, Physical and Engineering Sciences*, *366*, 705 - 728. https://doi.org/10.1098/rsta.2007.2123

Investigation of a multi-ball, automatic dynamic balancing mechanism for eccentric rotors

By K. Green†, A. R. Champneys, M. I. Friswell and A. M. Muñoz‡

Bristol Laboratory for Advanced Dynamics Engineering
University of Bristol, Queen's Building, University Walk
Bristol BS8 1TR, UK

This paper concerns an analytical and experimental investigation into the dynamics of an automatic dynamic balancer (ADB) designed to quench vibration in eccentric rotors. This fundamentally nonlinear device incorporates several balancing masses that are free to rotate in a circumferentially mounted ball race. An earlier study into the steady state and transient response of the device with two balls is extended to the case of an arbitrary number of balls. Using bifurcation analysis allied to numerical simulation of a fully nonlinear model, the question is addressed of whether increasing the number of balls is advantageous. It is found that it is never possible to perfectly balance the device at rotation speeds comparable with or below the first natural, bending frequency of the rotor. When considering practical implementation of the device, a modification is suggested where individual balls are contained in separate arcs of the ball race, with rigid partitions separating each arc. Simulation results for a partitioned ADB are compared to those from an experimental rig. Close qualitative and quantitative match is found between the theory and experiment, confirming that for sub-resonant rotation speeds, the ADB at best makes no difference to the imbalance, and can make things substantially worse. Further related configurations worthy of experimental and numerical investigation are proposed.

Keywords: Jeffcott rotor; imbalance; autobalancer; bifurcation; vibro-impact; multistability

1. Introduction

Imbalance in rotating machinery is a common source of vibration in many applications. Due to the centre of mass of the rotating component not being located at the centre of rotation, such *eccentric rotors* undergo periodic oscillation known as *whirl* (Jeffcott 1919). To limit this vibration, rotors are typically balanced by either using fixed static masses added to the rotor, or conversely by machining away small mass from the rotor, during the manufacturing process. However, such

† Present address: Theoretical Physics, FEW, Vrije Universiteit, De Boelelaan 1081, 1081HV Amsterdam, The Netherlands.

‡ Also: Escuela Técnica Superior de Ingenieros, University of Seville, Camino de los Descubrimientos s/n Sevilla 41092, Spain.

balancing cannot compensate for changes in imbalance that occur post production or as a result of operating conditions. Thus, frequent field balancing is required in many applications. Furthermore, this addition (subtraction) of static mass cannot account for a dynamic imbalance. One example of a dynamic imbalance is found in a washing machine, i.e., one cannot predict, a priori, where the washing will accumulate during the wash cycle (Adolfsson 2001).

Such dynamic imbalance has inspired the use of self-compensating, automatic dynamic balancing (ADB) mechanisms for eccentric rotors. The principle idea behind the ADB is that the balancing balls are subjected to a *driving force* caused by an *apparent* centripetal force acting from the off-set centre of mass to each ball. When the speed of rotation is below the first resonance, this driving force pushes the balls towards the imbalance. Therefore, moving the centre of mass away from the centre of rotation. However, when the speed of rotation is greater than the first resonance, the driving force pushes the balls to the opposite side of the rotor than the imbalance, thus moving the centre of mass towards the centre of rotation. Viscous damping in the ball race causes energy dissipation, allowing the balls to come to rest in asymptotically stable steady state positions.

The ADB first received attention as early as 1904, with the first theoretical investigation, accompanied by some experiments, undertaken by Thearle (1932). In this paper, there is also a discussion on why an ADB consisting of a fluid, in place of solid weights, would not work. Further theoretical investigations can be found in, e.g., (Majewski 1987; Sharp 1975), in which the results of a linear stability analysis show that complete balance is possible for sufficiently high rotation speeds. There are several commercial implementations of ADBs, with a number of patents granted from 1961 onwards; see (Lee & Van Moorhem 1996). Applications include optical disc drives, in which the aim is to achieve higher operating speeds without losing tracking performance (Kim & Chung 2002; van de Wouw et al. 2005), and balancing of machine tools, such as lathes, angle grinders and cutting tools (Rajalingham & Rakheja 1998). However, the ADB idea has not been more generally adopted, not least because the problem is fundamentally nonlinear, and is extremely sensitive to perturbation. Thus, while the ADB can completely quench whirl oscillations at some rotation speeds and for some initial conditions, it can also make the imbalance significantly worse.

Only recently have fully nonlinear analyses of the autobalancer been undertaken. Based on a Lagrangian description of the equations of motion, steady state bifurcation studies were carried out by Chung & Ro (1999) and by Adolfsson (2001), who identified regions in parameter space where stable rotating states, whether balanced or not, are possible. By moving to a rotating frame, Green et al. (2006a) carried out a detailed nonlinear investigation in the case of two balls, by computing both isolated branches of periodic solutions, and those emanating from Hopf bifurcations of the equilibrium states. Significant regions of bistability were found between these steady and periodic states, chaotic states, and states in which the balls rotate at a different angular frequency than the rotor. Furthermore, perturbations were shown to result in a large growth in the vibration before subsequent transient decay. This prompted the study by Green et al. (2006b), where the authors used the concept of pseudospectra to analyse this sensitivity to perturbation. It was found there that while the completely balanced state becomes increasing stable for high

rotation frequencies, it also becomes increasingly sensitive to perturbation, with an increasingly larger transient response before settling to the steady state.

Experimental investigations into the use of ADBs can be found in (Huang et al. 2002; Lee & Van Moorhem 1996; van de Wouw et al. 2005). One of the crucial issues is to design a releasing mechanism for the balancing masses that overcomes a global instability identified in Green (2005), in which the constant speed of the balancing masses lags that of the rotor. This may be partially overcome by clamping the balls in fixed positions until the desired, constant speed of rotation is reached. The balls could then be released at the same speed as the rotor. Van der Wouw et al. (2005) investigate a different mechanism with many balls in which the energy is dissipated through frictional forces between the balls and the race, which encourages the balls to remain approximately in phase with the rotor. However, a non-zero force is produced when the balls come to rest. Consequently, the steady state positions are not discrete but instead are found over small ranges of the race. This phenomenon is known as *stiction*. Thus, compared to the viscous damping case, this multiplicity of equilibria is harder to analyse and is more likely to produce a non-zero radial vibration when the balls come to rest.

The aim of this paper is to look at the practical issues associated with an implementation of the ADB on a large-scale rotor. We first consider the effect of using more than two balancing masses. In particular, we show how the stability regions found in Green et al. (2006a) for the two ball case change for three and four balls. We have also designed and built an experimental rig inspired by some of the previous experimental results. To overcome some of the observed instabilities we propose a novel design consisting of a partitioned ball race. However, for our chosen design we found that the dramatic increase in radial vibration meant that it was not practically possible to break through the first resonance. This set-back was also identified in (Lee & Van Moorhem 1996). Therefore, in this paper, our experimental investigations will be confined to the case of low rotation speeds.

The rest of the paper is organised as follows. In §2 we recall the equations of motion derived in Green et al. (2006a) of an eccentric rotor fitted with an ADB consisting of an arbitrary number of balancing balls. From direct analysis of the equations, we identify all possible steady state solutions, whether balanced or not, and show that the balanced state has a translational degeneracy for more than two balls. Next, in §3 we perform a full nonlinear bifurcation analysis for an ADB with three and four balancing balls, mapping out regions of stable equilibria as parameters in the problem are varied. This is complemented by simulation results obtained by numerical integration. In §4 we introduce the partitioned ball race model and show the results of numerical simulations. In §5 and §6 we describe our experimental set-up and present results which are compared with numerical simulation results for the corresponding parameter values, where only the experimental viscous damping coefficient has to be identified through fitting. Finally, in §7 we draw conclusions and suggest avenues for future work.

2. Automatic dynamic balancer

An automatic dynamic balancer consists of two or more balancing masses (balls) that are free to move in a ball race that is mounted at a fixed radial distance R from the center of rotation of a rotor. An eccentric rotating disc fitted with a partitioned

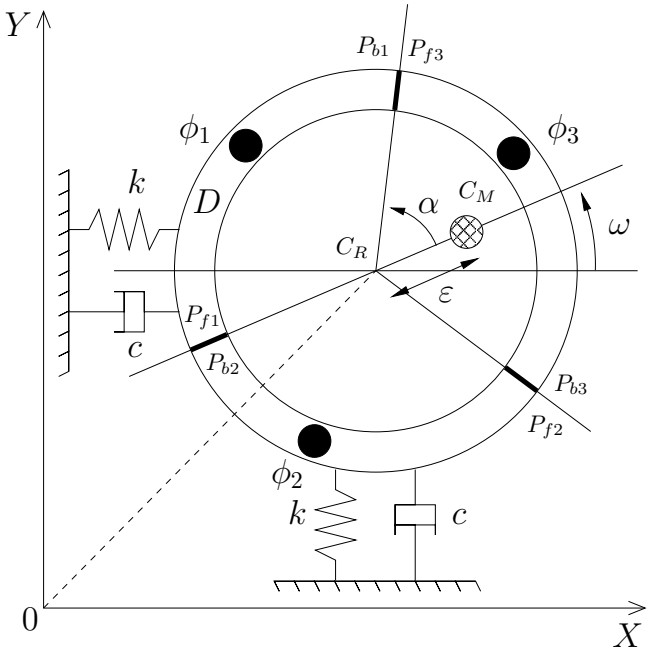

Figure 1. Schematic diagram of an automatic dynamic balancer with a partitioned race; see text for explanation of symbols.

ADB is shown schematically in figure 1 for the case of three balls, where for the time being we shall ignore the presence of the boundaries between partitions $P_{fi,bi}$ $(i = 1, 2, 3)$.

The race is positioned at a fixed distance from the center of rotation of the disc and contains a small amount of viscous fluid. The point C_M represents the centre of mass of the disc without the balancing masses. It is located at a distance (eccentricity) ε from the centre of rotation C_R. The whole rig (rotor plus ADB) is assumed to be isotropically suspended and to rotate at a constant angular velocity ω. Furthermore, all movement is assumed to be constrained to the horizontal (X, Y)-plane, and due to centrifugal forces, the balls are assumed to remain in contact with the race.

(*a*) *Equations of motion*

The equations of motion describing the ADB can be derived using a Lagrangian approach, with generalised coordinates

$$(X, Y, \phi_1, \phi_2, ..., \phi_n) \tag{2.1}$$

describing the motion of the rotor in the (X, Y)-plane, and the angular position of the ith ball, respectively. With the addition of a simple Raleigh dissipation function representing directly proportional viscous damping in both the ball race and the

rotor suspension system, one obtains

$$M\ddot{X} - M\varepsilon\omega^2\cos\omega t + \sum_{i=1}^{n} m\Big\{\ddot{X} - R\ddot{\phi}_i\sin(\omega t+\phi_i) - R(\omega+\dot{\phi}_i)^2\cos(\omega t+\phi_i)\Big\} + kX = -c\dot{X}, \tag{2.2}$$

$$M\ddot{Y} - M\varepsilon\omega^2\sin\omega t + \sum_{i=1}^{n} m\Big\{\ddot{Y} + R\ddot{\phi}_i\cos(\omega t+\phi_i) - R(\omega+\dot{\phi}_i)^2\sin(\omega t+\phi_i)\Big\} + kY = -c\dot{Y}, \tag{2.3}$$

and

$$-mR\Big[\ddot{X}\sin(\omega t+\phi_i) - \ddot{Y}\cos(\omega t+\phi_i)\Big] + mR^2\ddot{\phi}_i = -D\dot{\phi}_i. \tag{2.4}$$

In this formulation, it is assumed that all balls in the balancer have the same mass m and they all exert the same viscous drag D. The rotor, of mass M and radius R, is assumed to be driven at a constant angular velocity ω and to be isotropically mounted with spring constant k, damping coefficient c.

(*b*) *Dimensionless form in a rotating frame*

In dimensionless form, the parameters describing the system are: the rotation speed Ω, the external damping ratio ζ, the internal damping β, the mass ratio μ, and the eccentricity δ. These are given as

$$\Omega = \frac{\omega}{\omega_n},\ \zeta = \frac{c}{2\sqrt{kM}},\ \beta = \frac{D}{mR^2\omega_n},\ \mu = \frac{m}{M},\ \delta = \frac{\varepsilon}{R}, \tag{2.5}$$

where ω_n is the natural frequency of the system, given by

$$\omega_n = \sqrt{\frac{k}{M}}. \tag{2.6}$$

We note that, when deriving the following equations of motion, the displacements x and y were rescaled with respect to the radius R, and time rescaled with respect to the natural frequency ω_n.

Our final transformation converts the equations of motion to autonomous equations. We move the frame of reference to the rotating frame using the following substitutions:

$$X = x\cos(\Omega t) - y\sin(\Omega t), \tag{2.7}$$

$$Y = x\sin(\Omega t) + y\cos(\Omega t). \tag{2.8}$$

This leads to the following autonomous dynamical system describing the motion of the rotor and ADB in the x and y directions

$$\begin{aligned}&\begin{pmatrix} 1+n\mu & 0 \\ 0 & 1+n\mu \end{pmatrix}\begin{pmatrix} \ddot{x} \\ \ddot{y} \end{pmatrix}+\begin{pmatrix} 2\zeta & -2\Omega(1+n\mu) \\ 2\Omega(1+n\mu) & 2\zeta \end{pmatrix}\begin{pmatrix} \dot{x} \\ \dot{y} \end{pmatrix}\\ &+\begin{pmatrix} K & -2\Omega\zeta \\ 2\Omega\zeta & K \end{pmatrix}\begin{pmatrix} x \\ y \end{pmatrix}\\ &=\begin{pmatrix} \delta\Omega^2 \\ 0 \end{pmatrix}+\mu\sum_{i=1}^{n}\begin{pmatrix} (\Omega+\dot{\phi}_i)^2 & \ddot{\phi}_i \\ -\ddot{\phi}_i & (\Omega+\dot{\phi}_i)^2 \end{pmatrix}\begin{pmatrix} \cos\phi_i \\ \sin\phi_i \end{pmatrix}, \end{aligned} \tag{2.9}$$

and the motion of the i th ball,

$$\ddot{\phi}_i+\beta\dot{\phi}_i-(\ddot{x}-\Omega^2x-2\Omega\dot{y})\sin\phi_i+(\ddot{y}-\Omega^2y+2\Omega\dot{x})\cos\phi_i=0, \tag{2.10}$$

where ϕ_i measures the angular position of the ith ball from the line of eccentricity (C_R–C_M in figure 1); $i=1,..,n$. Furthermore, $K=1-\Omega^2(1+n\mu)$ represents the effect of centripetal acceleration. This reduces the effective stiffness of the system and is often called 'spin softening' or 'centripetal softening'. For a full derivation, including the procedure of making these equations dimensionless, we refer to (Green et al. 2006a).

(*c*) *Steady state analysis*

Green et al. (2006a) contains a detailed bifurcation analysis of steady states and periodic solutions found in an ADB with two balancing balls. In this paper, we will consider an ADB with three and four balls showing how this affects the potential stability of the system.

Steady state solutions are obtained by setting the time derivatives in (2.9) and (2.10) to zero. The steady state solution can be categorised as balanced, when $r=\sqrt{x^2+y^2}=0$, or unbalanced, when $r=\sqrt{x^2+y^2}\neq 0$ but the balls come to rest.

A balanced steady state corresponds to the centre of mass of the system being located at the centre of rotation, and satisfies

$$\begin{aligned} &x=y=0,\\ &\sum_{i=1}^{n}\cos\phi_i=-\frac{\delta}{\mu},\\ &\sum_{i=1}^{n}\sin\phi_i=0. \end{aligned} \tag{2.11}$$

When $n>2$, there exist infinitely many solutions to (2.11). We will refer to these solutions as the sets of balanced states **1**.

As is the case for two balls, unbalanced steady states are found when

$$\frac{y}{x}=\tan\phi_i, \quad i=1...n, \tag{2.12}$$

with solutions

$$\phi_i=\phi_1+k_i\pi, \quad i=2...n,\ k_i\in\mathbb{Z}. \tag{2.13}$$

Without loss of generality, we consider $k_i = 0$ or 1. When $k_i = 0$, the first and the ith ball coincide, and when $k_i = 1$, the first and the ith ball are found on opposite sides of the race to each other, in line with the centre of rotation C_R. We note that in this analysis, collisions between balls are neglected. Physically, this could be realised by considering a multiple ball race (Hwang & Chung 1999).

When all balls coincide ($k_i = 0$), solutions, in terms of ϕ_1, are,

$$\begin{aligned} x &= \frac{K\Omega^2(n\mu\cos\phi_1 + \delta) + 2n\mu\Omega^3\zeta\sin\phi_1}{K^2 + (2\Omega\zeta)^2}, \\ y &= \frac{nK\mu\Omega^2\sin\phi_1 - 2\Omega\zeta(\delta\Omega^2 + n\mu\Omega^2\cos\phi_1)}{K^2 + (2\Omega\zeta)^2}, \end{aligned} \tag{2.14}$$

where

$$\begin{aligned} \phi_1 &= \pm\arccos\left(\frac{-2n\mu\Omega\zeta}{\delta\sqrt{K^2 + (2\Omega\zeta)^2}}\right) - \arctan\left(\frac{-K}{2\Omega\zeta}\right), \\ \phi_i &= \phi_1, \quad i = 2...n. \end{aligned} \tag{2.15}$$

In what follows, we will refer to (2.14) and (2.15) as the *coincident state* $\mathbf{2}^{\pm}$.

When $(n-m)$ balls lie opposite from m coincident balls ($k_i = 1$ for some i), we find solutions

$$\begin{aligned} x &= \frac{K\Omega^2((2m-n)\mu\cos\phi_1 + \delta) + 2(2m-n)\mu\Omega^3\zeta\sin\phi_1}{K^2 + (2\Omega\zeta)^2}, \\ y &= \frac{(2m-n)K\mu\Omega^2\sin\phi_1 - 2\Omega\zeta(\delta\Omega^2 + (2m-n)\mu\Omega^2\cos\phi_1)}{K^2 + (2\Omega\zeta)^2}, \end{aligned} \tag{2.16}$$

where

$$\begin{aligned} \phi_1 &= \pm\arccos\left(\frac{-2(2m-n)\mu\Omega\zeta}{\delta\sqrt{K^2 + (2\Omega\zeta)^2}}\right) - \arctan\left(\frac{-K}{2\Omega\zeta}\right), \\ \phi_i &= \phi_1, \quad i = 2...m, \\ \phi_j &= \phi_1 + \pi, \quad j = m{+}1...n. \end{aligned} \tag{2.17}$$

In what follows, we will refer to (2.16) and (2.17) as the $(n-m)$ *in-line states* $\mathbf{3(n\text{-}m)}^{\pm}$.

Again, we refer to Green et al. (2006a) for an analysis of two balls, i.e., $n = 2$ and consequently, in (2.16) and (2.17), $m = 1$. Here we consider three and four balancing balls.

For $n = 3$, we can either have $m = 1$ or $m = 2$. However, as the balls are identical so are these states, i.e., at any one time we have one separate and two coincident balls. The sign of (2.17) determines where the separate (or the coincident) ball(s) are with respect to the imbalance. Hence we refer to the in-line states, with three balls, simply as $\mathbf{3}^{\pm}$.

For $n = 4$, we have three situations, one where two balls are coincident ($m = 2$) and one where three balls are coincident ($m = 3$). (The latter state being identical to $m = 1$.) We will refer to these four-ball, in-line states as **3A** and $\mathbf{3B}^{\pm}$, respectively.

(*d*) *Conditions for existence of steady states*

Analogous to the two-ball case, (2.11) implies that, for a balanced state **1** to exist,

$$\mu \geq \mu_c := \frac{\delta}{n}. \tag{2.18}$$

In other words, to achieve balance, the combined mass of the balls must be large enough to cope with the eccentricity δ. Note that when equality is reached, this corresponds to a coincident state $\mathbf{2}^{\pm}$.

The coincident states $\mathbf{2}^{\pm}$ exist only if the modulus of the argument of the inverse cosine of (2.15) is less than unity, i.e.,

$$K^2 > (2\Omega\zeta)^2 \left(\left(\frac{n\mu}{\delta} \right)^2 - 1 \right). \tag{2.19}$$

As for the two-ball case, when $\mu < \mu_c$, the states $\mathbf{2}^{\pm}$ always exist.

Likewise, from (2.17), the in-line states $\mathbf{3(n\text{-}m)}^{\pm}$ exist if

$$K^2 > (2\Omega\zeta)^2 \left(\left(\frac{(2m-n)\mu}{\delta} \right)^2 - 1 \right). \tag{2.20}$$

In other words, they exist for $\mu < \delta(2m - n)$.

The existence of the coincident and the in-line states, above the critical values of μ depends on the other parameters δ, ζ and β in a non-trivial way. To investigate this we turn to numerical bifurcation techniques.

3. Numerical results for multiple balls

In this section we investigate the stability of the steady states identified in §2c using numerical bifurcation techniques. Namely, we compute the boundaries between solutions with differing stability using the continuation package `MATCONT` (Dhooge et al. 2004). In this way, a detailed map is produced showing how regions of stability change as parameters are varied. These results will be backed up by direct simulation of the equations of motion.

In each case, where appropriate, the fixed parameters are given as

$$\beta = \delta = \zeta = 0.01, \ \mu = 0.05. \tag{3.1}$$

These parameters were chosen to allow direct comparison with the two ball ADB study of Green et al. (2006a).

(*a*) *Steady state bifurcation diagram for* $n = 3$

We start by investigating the ADB with three balancing balls. Figures 2(a)–(d) show two-parameter bifurcation diagrams for Ω versus μ, δ, ζ, and β, respectively. The dark, shaded regions of figure 2 indicate regions of parameter space in which the balanced state **1** is stable. The lighter shaded regions correspond to parameters at which one of the coincident states $\mathbf{2}^{\pm}$ is stable. No shading corresponds to regions

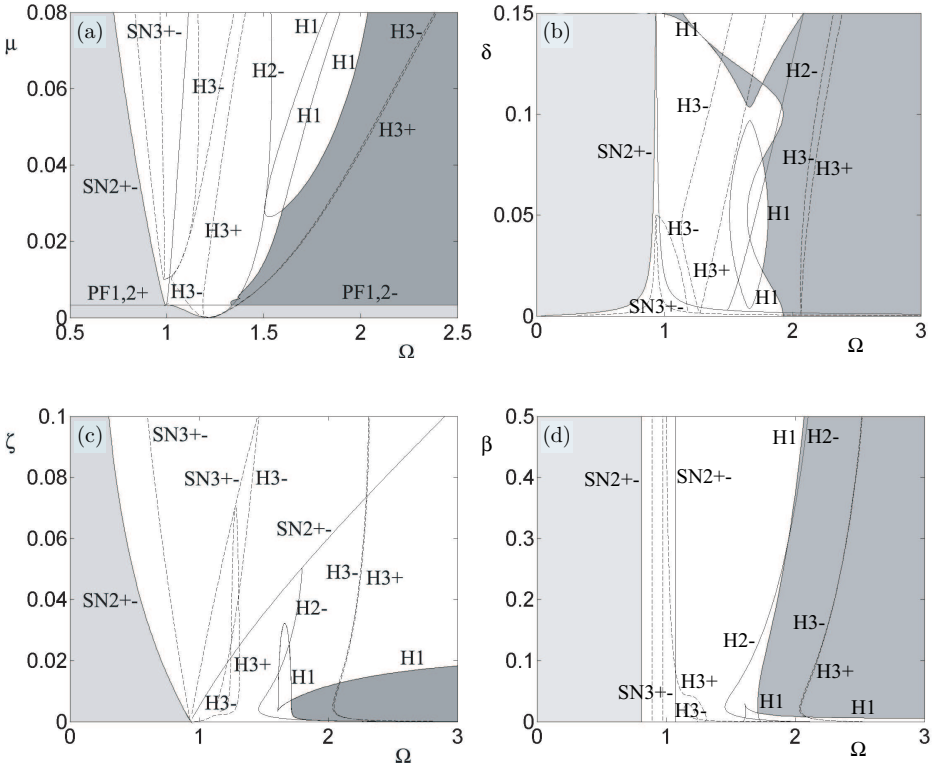

Figure 2. Two-parameter bifurcation diagrams of steady state solutions in the three ball ADB.

(Solid lines correspond to saddle-node bifurcations SN and Hopf bifurcations H of states **1** and **2**±. Similarly, broken lines correspond to bifurcations of state **3**. Dark shaded regions correspond to a stable state **1** and light shaded regions to a stable state $\mathbf{2}^-$. When fixed, the parameters are $\beta = \delta = \zeta = 0.01$ and $\mu = 0.05$. The varying parameters are Ω versus μ (a), Ω versus δ (b), Ω versus ξ (c), and Ω versus β (d).)

of instability. Solid lines correspond to bifurcations of states **1** and $\mathbf{2}^{\pm}$, while dashed lines correspond to bifurcations of states $\mathbf{3}^{\pm}$. The curves are labeled as Hopf bifurcations 'H' (oscillatory instabilities) which occur when a pair of pure imaginary eigenvalues cross the imaginary axis, and saddle-node bifurcations 'SN' (steady state instabilities, which due to symmetry are actually pitchfork bifurcations for some of the states). In the latter case, a real eigenvalue crosses the imaginary axis (Kuznetsov 1997). Furthermore, as there are infinitely many balanced states, we fix $\phi_3 = \pi$ when analysing the bifurcations of state **1**. This is equivalent to computing bifurcations of state **1** for the two-ball case with a different δ to that used in Green et al. (2006a). Likewise, the coincident states may be compared to a two ball case where the mass of the balls are increased, and the in-line states to the case when the each ball has a different mass.

It is clear from these bifurcation diagrams that for low rotation speeds a coincident state $\mathbf{2}^{\pm}$ is stable. Specifically, it can be shown that this is state $\mathbf{2}^-$. While

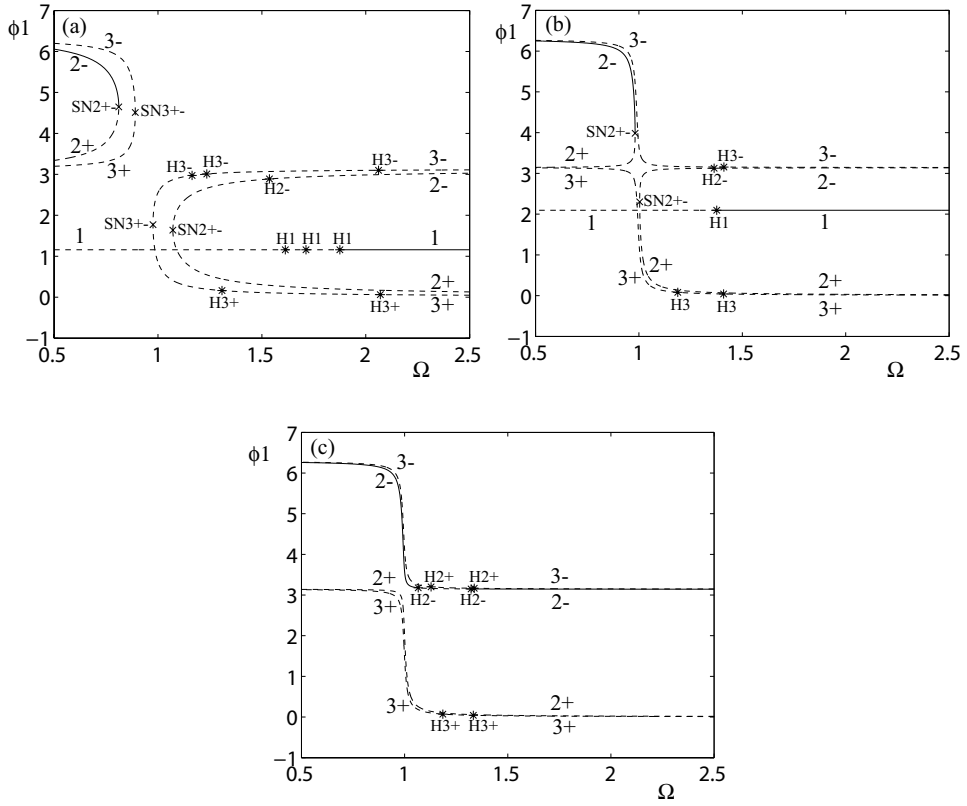

Figure 3. One parameter bifurcation diagrams for the three ball ADB.

(Panels (a), (b) and (c) show diagrams for Ω versus ϕ_1 for $\mu = 0.05$, 0.005 and 0.0025, respectively. Solid lines correspond to stable states and broken lines to unstable states, the numbers indicating the type of state. Saddle-node bifurcations are denoted by a ($\times$) and Hopf bifurcations by a ($*$).)

for high rotation speeds the balanced state **1** is shown to be stable. Furthermore, figure 2(b) shows a region of stability, for high eccentricity δ, of the balanced state **1**, close to the resonant rotation speed $\Omega = 1$. This is our first indication that the addition of more balancing balls changes the stability properties. We recall that in Green et al. (2006a), the two ball ADB was shown to exhibit a small region of stability close to this resonant speed for all parameters. Moreover, it was shown that this small region of stability was only accessible through a very limited range of initial conditions. In other words, for intermediate rotations speeds, and random initial conditions, the system is likely to be drawn into unstable, possibly chaotic dynamics. However, the three ball ADB shows little stability close to the resonant speed, for the parameter range under consideration. Finally, in the (Ω, μ)-plane and for low values of μ, a coincident state $\mathbf{2}^{\pm}$ is stable. Again, it can be shown that this is state $\mathbf{2}^{-}$.

Moreover, for each of the parameter sets under consideration, and starting within a region of balanced equilibrium (dark shading) the following scenario holds:

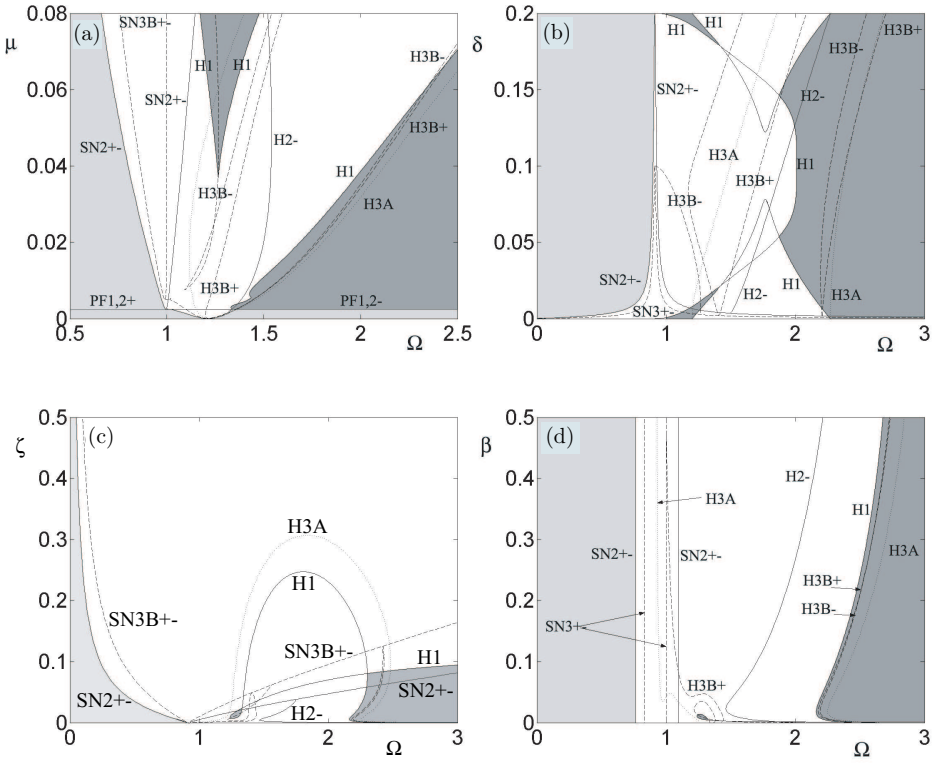

Figure 4. Bifurcation diagram of steady state solutions in the four ball ADB.

(Solid lines correspond to saddle-node bifurcations SN and Hopf bifurcations H of states **1** and **2**±. Similarly, broken lines correspond to bifurcations of state **3**. Dark shaded regions correspond to a stable state **1** and light shaded regions to a stable state $\mathbf{2}^-$. When fixed, the parameters are $\beta = \delta = \zeta = 0.01$ and $\mu = 0.05$. The varying parameters are Ω versus μ (a), Ω versus δ (b), Ω versus ξ (c), and Ω versus β (d).)

For decreasing Ω, the balanced state **1** is destabilised in a Hopf bifurcation H1. The dynamics then enter a region of non-steady state behaviour, containing periodic oscillations through to chaotic motion. Decreasing Ω further sees a saddle-node bifurcation SN2±. At this point, the two coincident states $\mathbf{2}^\pm$ are born. Again, we have that the state $\mathbf{2}^-$ is stable, while the state $\mathbf{2}^+$ is unstable.

Figure 2(c) shows that the region of stability of the balanced state **1** in the (Ω, δ)-plane is small. This is again in stark contrast with the two ball case in which this region of stability was seen to cover approximately half of the parameter plane under consideration. This shows that increasing the number of balancing masses has a detrimental effect on whether or not stability can be achieved for the range of parameters under consideration. Physically, this implies that the three ball ADB cannot achieve balance when the rotor damping ζ is too high. We note that the bifurcation diagram in the (Ω, β)-plane is practically identical to the two ball case.

Like the two ball case, the state $\mathbf{3}^\pm$ was found to always be unstable. However, it is involved in an interesting bifurcation scenario. Figures 3(a) to (c) show one-

parameter bifurcation diagrams, for the three ball ADB, for $\mu = 0.05$, 0.005 and 0.0025, respectively, i.e., for an increasing rotor mass to ball mass ratio. For large μ, figure 3(a) shows that the four states $\mathbf{2}^{\pm}$ and $\mathbf{3}^{\pm}$ are born in two separate saddle-node bifurcations. These occur at the left and right edges of the 'v'-shaped curves SN2± and SN3± shown in figure 2(a). Decreasing μ sees one pass the base of the 'v' representing the saddle-node curve SN3± while still inside the 'v'-shaped curve SN2±; see figure 2(a). Figure 3(b) shows a one-parameter transition at such a value of μ, namely, $\mu = 0.005$. It is clear that the two sets of states $\mathbf{2}^{\pm}$ are still born in two separate saddle-node bifurcations SN2±. However, the two sets of states $\mathbf{3}^{\pm}$ have now merged into two curves; a lower curve on which one finds $\mathbf{3}^{+}$ and an upper curve on which one finds $\mathbf{3}^{-}$. The states $\mathbf{3}^{\pm}$ now exist for all Ω. Finally, figure 3(c) shows that decreasing μ further to $\mu = 0.0025$ we pass the base of the 'v' representing the saddle-node curve SN2±; again see figure 2(a). Like the case for the states $\mathbf{3}^{\pm}$, the sets of states $\mathbf{2}^{\pm}$ merge together. They form an upper curve consisting of $\mathbf{2}^{-}$ and a lower curve consisting of $\mathbf{2}^{+}$. Subsequently, for low values of μ, both the states $\mathbf{2}^{\pm}$ and $\mathbf{3}^{\pm}$ exist for all Ω.

(*b*) *Steady state bifurcation diagram for* $n = 4$

Figures 4(a) to (d) show two-parameter bifurcation diagrams for the four ball ADB. The notation used is the same as for the three ball diagrams of figure 2. The exception being that the inline state **3** now comes in two varieties: **3A** and $\mathbf{3B}^{\pm}$; recall §2c. Again, as there are infinitely many balanced states **1**, we fix $\phi_3 = \pi$ and $\phi_4 = -\pi$ when computing bifurcations of state **1**. Once more, the balanced state **1** is shown to be stable for high rotation speeds, while the coincident state $\mathbf{2}^{-}$ is stable for low rotation speeds or low mass ratios μ. Interestingly, however, the region of stability around the resonant speed ($\Omega = 1$), identified for the two ball ADB in Green et al. (2006a) but shown to disappear for the three ball ADB in figure 2(a) above, reappears for the four ball ADB. In fact, figure 4(b) shows that this region of stability now occurs for both low and high values of δ. It is clearly seen that all regions of stability of state **1** are connected to the Hopf curve H1. (In fact, the regions of stability of state **1** are connected by this curve for large values of μ in all panels of figure 4.)

Figure 4(c) shows that upon increasing the number of balls, the region of stability of state **1** in the (Ω, δ)-plane shrinks further. Moreover, the region of stable operation of state $\mathbf{2}^{-}$, for low rotation speeds, is also shown to decrease in size. The unshaded region of instability is shown to dominate the (Ω, δ)-plane. Finally, again, figure 4(d) shows little quantitative change in the stability structure of the (Ω, β)-plane. However, the large region of stability of state **1** does move further to the right. In other words, increasing the number of balls, is again shown to increase the size of the region of instability.

We note that the states **3A** and $\mathbf{3B}^{\pm}$ are always unstable. The interesting bifurcation scenario outlined in figure 3 occurs again for the four ball ADB.

(*c*) *Numerical simulation results*

We now present results obtained by numerical integration of the system (2.9) and (2.10). We restrict ourselves to the case of 3 balls only, in order to illustrate the extra

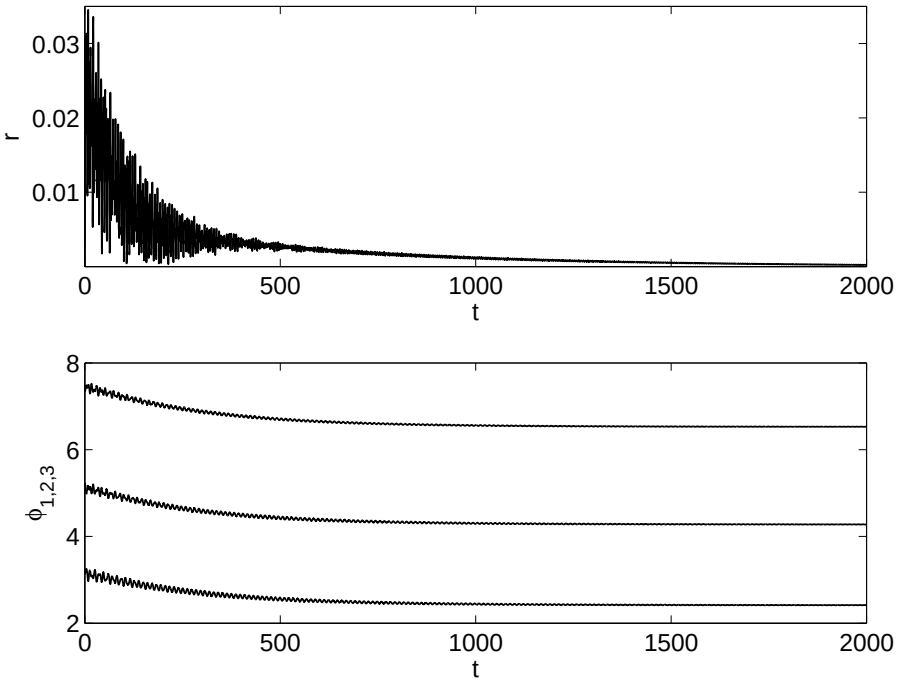

Figure 5. Time evolution of an ADB with 3 balls for $\Omega = 2.5$.

(Other parameters were fixed at $\zeta = 0.01$, $\beta = 0.01$, $\delta = 0.01$ and $\mu = 0.05$. Panel (a) shows the radial vibration $r = \sqrt{x^2 + y^2}$, while panel (b) shows the ball positions $\phi_{1,2,3}$, against time t. Initial conditions were fixed at $x = y = \dot{x} = \dot{y} = 0$, $\dot{\phi}_1 = \dot{\phi}_2 = \dot{\phi}_3 = 0$, $\phi_1 = \pi/3$, $\phi_2 = \pi$ and $\phi_3 = 5\pi/3$.)

complexity of having degenerate equilibria when $n > 2$. Our aim is merely to show the different steady states identified in §2. A complete transient analysis, including multistability between steady states and possible periodic states, emanating from the Hopf bifurcations identified above, is beyond the scope of this study.

Figure 5 shows the time evolution of the radial vibration $r = \sqrt{x^2 + y^2}$ (a), and the angular position of each of the three balancing balls $\phi_{1,2,3}$ (b). Initial conditions were taken such that one ball was launched directly opposite to the imbalance, with the other two launched from symmetric positions at a angular distance of $\pi/3$ from the imbalance. Namely, $\phi_1(0) = \pi/3$, $\phi_2(0) = \pi$ and $\phi_3(0) = 5\pi/3$. Note that if the balls were clamped in this way during an acceleration phase, they would not add to the imbalance. Parameters were fixed at $\Omega = 2.5$, $\zeta = 0.01$, $\beta = 0.01$, $\delta = 0.01$ and $\mu = 0.05$. As identified in figure 2 the radial vibration is seen to go to zero. In other words, the ADB has balanced the eccentric rotor.

Figure 6 shows the time evolution of r and $\phi_{1,2,3}$ for $\Omega = 0.5$, $\zeta = 0.01$, $\beta = 0.01$, $\delta = 0.01$ and $\mu = 0.05$. Again, the balls were initially fixed at $\phi_1(0) = \pi/3$, $\phi_2(0) = \pi$ and $\phi_3(0) = 5\pi/3$. It is clearly seen that, for these parameters, the balls converge to the same angular position. This is the coincident state predicted in figure 2.

Finally, figure 7 shows the dynamics for $\Omega = 1.6$. All other parameters and initial conditions remain unchanged. For this value of Ω, figure 2 predicts no stable dynamics. This is clearly seen in figure 7. The radial vibration r exhibits chaotic

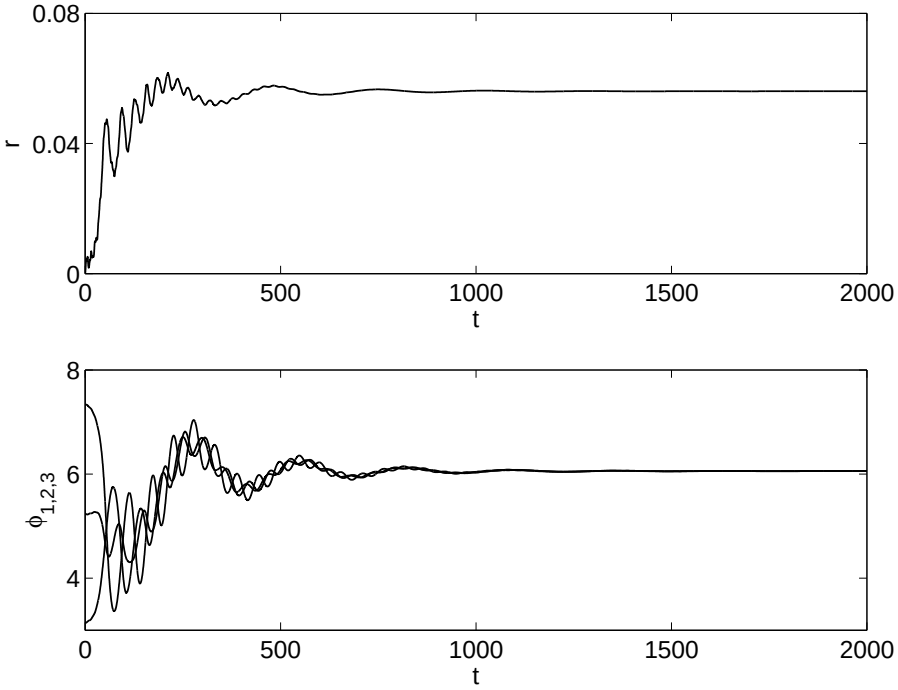

Figure 6. Time evolution of an ADB with 3 balls $\Omega = 0.5$.

(Other parameters were fixed at $\zeta = 0.01$, $\beta = 0.01$, $\delta = 0.01$ and $\mu = 0.05$. Panel (a) shows the radial vibration $r = \sqrt{x^2 + y^2}$, while panel (b) shows the ball positions $\phi_{1,2,3}$, against time t. Initial conditions were fixed at $x = y = \dot{x} = \dot{y} = 0$, $\dot{\phi}_1 = \dot{\phi}_2 = \dot{\phi}_3 = 0$, $\phi_1 = \pi/3$, $\phi_2 = \pi$ and $\phi_3 = 5\pi/3$.)

dynamics (a), while the angular position of each ball is seen to continually decrease; a constant rotation modulo 2π (b). The speed of the imbalance has exceeded the average speed of each ball. In fact, as well as reaching a speed which lags that of the rotor, the positions of the balls are also undergoing chaotic motion. This is akin to the instability identified in Green (2005). We note that with two or more balls, one or more may undergo this instability while the rest maintain pace with the speed of the rotor; see figure 9(d) of Green et al. (2006a).

(*d*) *Discussion on optimal number of balls.*

The results obtained so far suggest that there is little advantage in increasing the number of balls in the ADB, purely in terms of the size of the parameter region in which the balanced state **1** is stable. For rotors whose rotation speeds are sufficiently beyond the fundamental resonance $\Omega = 1$, this issue is not so crucial and it is more important to assess the sensitivity of the balanced state to perturbations, and the size of its basin of attraction. Without repeating the detailed analysis in Green et al. (2006b) this aspect of the problem is not so clear for more balls, but preliminary computations suggest that the problem is more robust, i.e., the basin of attraction is larger, for high rotation speeds with an increased number of balls. Thus, at this

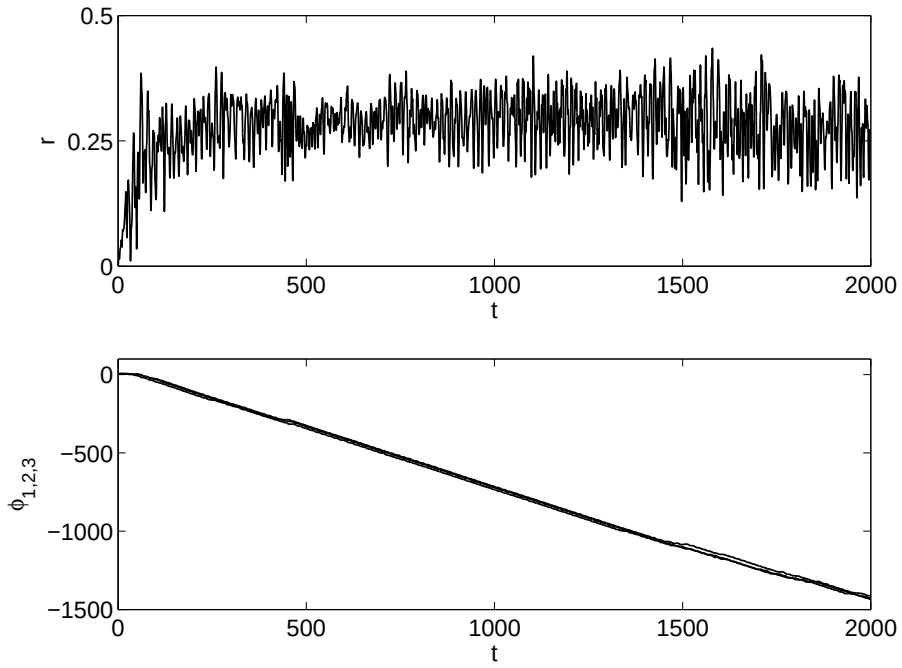

Figure 7. Time evolution of an ADB with 3 balls for $\Omega = 1.6$.

(Other parameters were fixed at $\zeta = 0.01$, $\beta = 0.01$, $\delta = 0.01$ and $\mu = 0.05$. Panel (a) shows the radial vibration $r = \sqrt{x^2 + y^2}$, while panel (b) shows the ball positions $\phi_{1,2,3}$, against time t. Initial conditions were fixed at $x = y = \dot{x} = \dot{y} = 0$, $\dot{\phi}_1 = \dot{\phi}_2 = \dot{\phi}_3 = 0$, $\phi_1 = \pi/3$, $\phi_2 = \pi$ and $\phi_3 = 5\pi/3$.)

stage there is no general conclusion possible on the optimum number of balls and the choice would depend on the specific details of the implementation of the ABD.

4. Partitioned ball race

Once the dynamics converge to the rotating state identified in figure 7, one cannot attain stability for higher rotation speeds simply by ramping up the speed. This instability may easily be reached through an acceleration phase, as identified in Green (2005), i.e., by increasing the rotation frequency through the resonant speed, which causes the balls to slip and thus have a speed less than that of the rotor. One solution to this problem would be to clamp the balls in fixed positions until the desired, constant speed of rotation is reached (Ernst 1951). The balls could then be released at the same speed as the rotor. Another solution, which we introduce here for the first time, is to place partitions in the ball race; dividing the race into *sectors* of equal arc-length, with one ball in each partition. During a rapid acceleration phase, the balls would be forced to rest against their lagging partition. After the acceleration, the balls would have the same speed as the rotor (from an external observer's point of view).

Intuitively, in order to achieve a balanced state it would seem necessary to have at least three partitions. In the case of two balls, there is no degeneracy (internal

degree of freedom) in the balanced equilibrium state. Hence, for certain positions of imbalance, the fixed partitions will not allow the balls to migrate to this equilibrium position. For three or more balls, we have an internal degree of freedom that allows balance to be achieved (at appropriate parameter values for which the state **1** exists) no matter where the partitions are placed with respect to the imbalance. Hence, in what follows we shall consider the case of three partitions exclusively.

A partitioned ball race has other potential advantages. Firstly, the coincident equilibrium state is not possible. This equilibrium results in an increased imbalance when it is stable, which is generally for sub-critical rotation speeds. The elimination of this state might lead to more favourable sub-critical behaviour. Another advantage is that collisions between balls (an effect we have not included in our model) cannot occur. Instead, we have collision between balls and partitions only, which can be designed to have specific desired properties leading to impacting behaviour with either high or low coefficients of restitution.

Figure 1 showed a schematic diagram of an ADB with such a partitioned race with three partitions $P_{fi,bi}$ $(i = 1, 2, 3)$. Here subscript b denotes the back (lagging) face and f the front (leading) face of a partition with respect to the direction of rotation. The equations of motion governing this system are the same as (2.9) and (2.10), together with the following impact law, modelling the collisions of the balls with their respective partitions:

$$\begin{aligned} &\text{if } \ \phi_i = \alpha + \frac{2(i-1)\pi}{n} + r_b \ \text{ or } \ \phi_i = \alpha + \frac{2i\pi}{n} - r_b, \\ &\text{then } \ \dot{\phi}_i \to -e\dot{\phi}_i, \ \ e \in [0,1], \ i = 1...n. \end{aligned} \tag{4.1}$$

Additional parameters include r_b: the angular diameter of the ball; α: the angle to the first partition from the line of imbalance (C_R to C_M); and a coefficient of restitution e. In other words, this law states that when a ball impacts with its partition, its direction of motion is reversed and its speed is multiplied by e.

To show that the dynamics are consistent with those identified in §3c, figure 8 shows the evolution of the radial vibration $r = \sqrt{x^2 + y^2}$ (a) and the angular positions of the balls (b), for $\Omega = 0.5$. After an acceleration phase, the initial conditions of the balls were fixed at $\phi_1(0) = \pi/3 + r_b$, $\phi_2(0) = \pi + r_b$ and $\phi_3(0) = 5\pi/3 + r_b$; $r_b = 0.14$. Parameters were fixed to coincide with those used in §3c. Namely, $\zeta = 0.01$, $\beta = 0.01$, $\delta = 0.01$ and $\mu = 0.05$. Additional parameters were fixed at $\alpha = \pi/3$ and $e = 0.001$. This small value of e was chosen to model the impact between the ball and the grub screw; the actual contact taking place near the top of the ball. In figure 8(b), the partitions are marked by grey dashed lines, and the position of the imbalance by a solid (grey) line (at $\phi_i = 2\pi$). For this low rotation speed, it is clear that the balls want to move to the coincident state $\mathbf{2}^{\pm}$ identified in figure 6. However, the partitions impede their progress. As expected this results in a lower radial vibration of $r \approx 0.032$ compared to $r \approx 0.056$; recall figure 6(a).

Figure 9 shows the dynamics for $\Omega = 1.6$. At this rotation speed, figure 7 identified the instability in which the speed of the balls lag that of the rotor. The partitions obviously stop such dynamics. Instead, the balls continuously impact between their leading and lagging partitions in a periodic manner. However, this bouncing motion has an alarming effect on the radial vibration, which increases above $r = 1$.

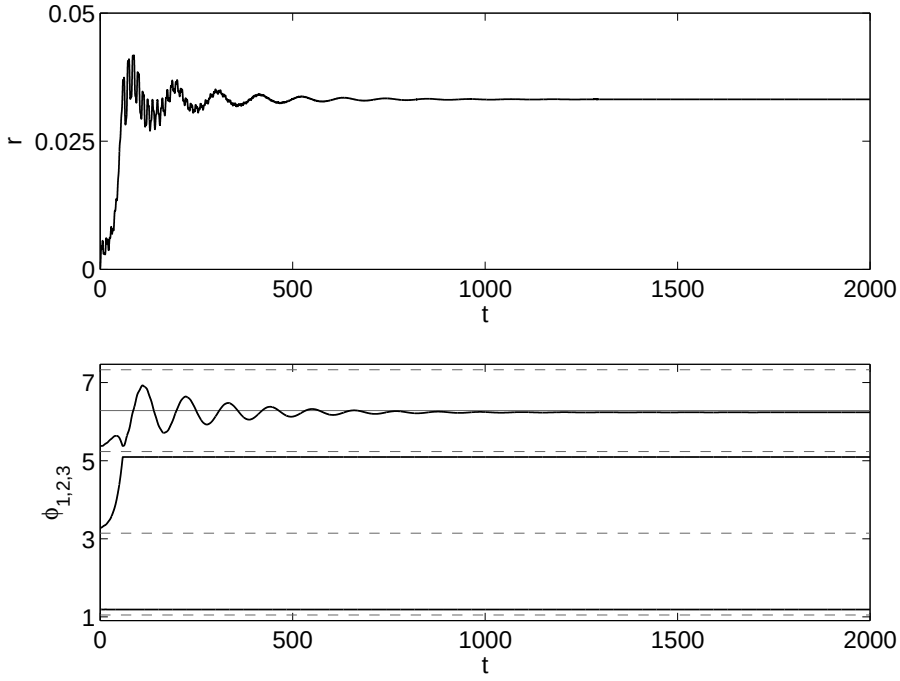

Figure 8. Time evolution of a partitioned ADB with 3 balls for $\Omega = 0.5$.
(Other parameters were fixed at $\zeta = 0.01$, $\beta = 0.01$, $\delta = 0.01$ and $\mu = 0.05$. Panel (a) shows the radial vibration $r = \sqrt{x^2 + y^2}$, while panel (b) shows the ball positions $\phi_{1,2,3}$, against time t. Initial conditions were fixed at $x = y = \dot{x} = \dot{y} = 0$, $\dot{\phi}_1 = \dot{\phi}_2 = \dot{\phi}_3 = 0$, $\phi_1 = \pi/3 + r_b$, $\phi_2 = \pi + r_b$ and $\phi_3 = 5\pi/3 + r_b$.)

Finally, figure 10 shows the dynamics for $\Omega = 2.5$. The system is clearly seen to balance; the radial vibration r goes to zero, while, after one impact with their respective leading partitions, the balls come to rest away from their partitions. Interestingly, the time it takes for the ADB to balance the rotor is far shorter than for the unpartitioned case; compare with figure 5.

5. Experimental results

In an attempt to verify our numerical results, we designed and built an eccentric rotor fitted with an ADB; see figure 11. This consisted of an aluminum rotor hub with a radius of 155 mm into which was machined a steel ball race centred at a radial distance of 105 mm. The total mass of the hub was 10 kg. Steel balls with a 30 mm diameter, 0.110 g mass were used as balancing masses. These balls were visible through a perspex covering, into which grub screws were sunk in order to form the partitions. An imbalance was added by attaching bolts to the extremity of the hub. The rotor was fitted midway along a silver steel shaft of diameter 30 mm. The effective length of the shaft could be varied by moving bearing supports situated above and below the rotor. The whole set-up was mounted vertically (so that gravitational effects could be neglected) and was driven by a variable speed D.C. motor, through a flexible coupling, fitted above the shaft.

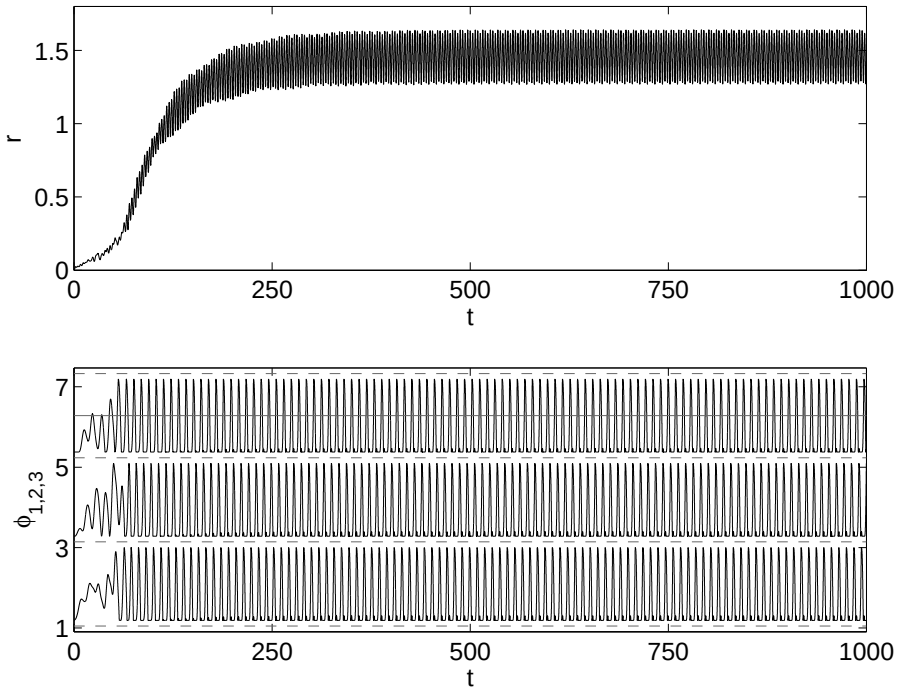

Figure 9. Time evolution of a partitioned ADB with 3 balls for $\Omega = 1.6$.

(Other parameters were fixed at $\zeta = 0.01$, $\beta = 0.01$, $\delta = 0.01$ and $\mu = 0.05$. Panel (a) shows the radial vibration $r = \sqrt{x^2 + y^2}$, while panel (b) shows the ball positions $\phi_{1,2,3}$, against time t. Initial conditions were fixed at $x = y = \dot{x} = \dot{y} = 0$, $\dot{\phi}_1 = \dot{\phi}_2 = \dot{\phi}_3 = 0$, $\phi_1 = \pi/3 + r_b$, $\phi_2 = \pi + r_b$ and $\phi_3 = 5\pi/3 + r_b$.)

In the results presented here a 100 g bolt was used as an imbalance. The bearing supports were fitted to provide an effective shaft length of 1.305 m. Furthermore, the ball race was coated with a thin layer of hydraulic fluid to provide some resistance to the movement of the balls against the race.

At rest, a modal analysis was performed using `LMS Test Lab` software to estimate the first resonance of the entire system. This was found to be $\omega_n = 29.5$ Hz. Using this first resonance, a half-power bandwidth method gave the external damping coefficient of the system as $c = 0.052$ Nsm^{-1}; while the spring coefficient of the shaft and rotor system was calculated as $k = 3.436 \times 10^{-5}$ Nm^{-1}. During rotation, a `Polytec` Doppler laser vibrometer was used to measure the vibration of the rotor and record the vibration spectra. Furthermore, a strobe light (shown in figure 11) and a video camera were used to visualise and record the ball positions. The speed of the rotor and the frequency of the strobe light were controlled using `dSpace` software.

(*a*) *Steady state ball configurations*

During our experimental investigations, in addition to the situation in which the balls were *fixed* in a symmetric configuration, so as to not add to the imbalance, we

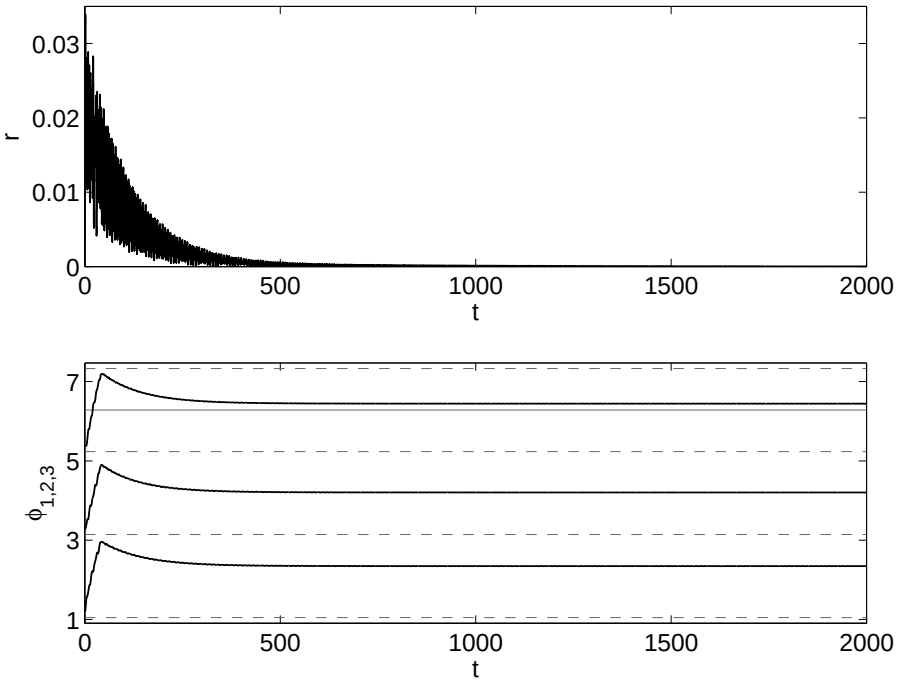

Figure 10. Time evolution of a partitioned ADB with 3 balls for $\Omega = 2.5$.

(Other parameters were fixed at $\zeta = 0.01$, $\beta = 0.01$, $\delta = 0.01$ and $\mu = 0.05$. Panel (a) shows the radial vibration $r = \sqrt{x^2 + y^2}$, while panel (b) shows the ball positions $\phi_{1,2,3}$, against time t. Initial conditions were fixed at $x = y = \dot{x} = \dot{y} = 0$, $\dot{\phi}_1 = \dot{\phi}_2 = \dot{\phi}_3 = 0$, $\phi_1 = \pi/3 + r_b$, $\phi_2 = \pi + r_b$ and $\phi_3 = 5\pi/3 + r_b$.)

identified two further, coexisting configurations in which the balls came to rest in the ADB.

Figure 12 shows these two configurations for a frequency of 10 Hz ($\Omega = 0.339$). The partitions are highlighted by crosses and the imbalance by a square. The positions of the balls are highlighted by large dots.

Figure 12(a) shows the first configuration, which we will refer to as *free*. Here, the ball closest to the imbalance moves furthest from its lagging partition P_{3b}. While the other two balls both move away from their lagging partitions; the ball directly opposite the imbalance moving furthest. Both balls come to rest in the ball race. This free-ball configuration was seen to be stable up to a rotation frequency of approximately 11.5 Hz ($\Omega = 0.390$). Furthermore, it was shown to be robust against external perturbation, namely, striking the shaft or the underside of the rotor with a hammer.

For frequencies above approximately 11.5 Hz the free-ball configuration was destabilised. The resulting position of the balls is shown in figure 12(b). It is clear that the balls move as far as possible towards the imbalance, as would be expected for sub-critical rotation speeds. This results in the ball closest to the imbalance coming to rest between the lower two partitions of figure 12, with the other two balls coming to rest against these two partitions. This configuration is analogous

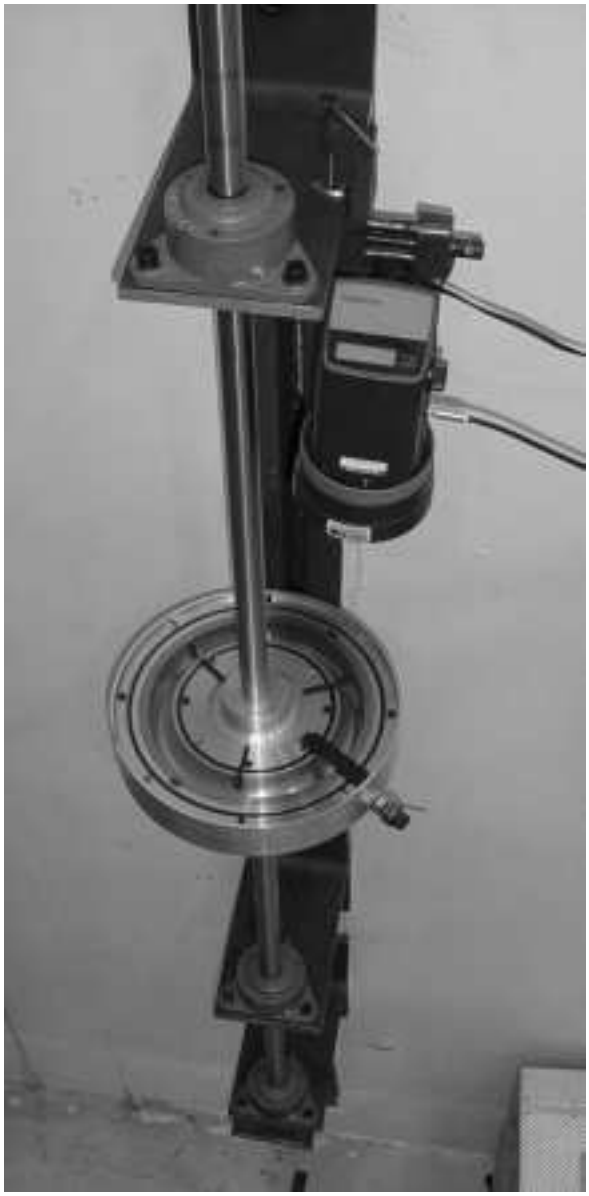

Figure 11. Experimental rig.

to the coincident steady state $\mathbf{2}^{\pm}$ identified in §2c and shown in figure 8. Hence, we will refer to this as the *coincident* ball configuration.

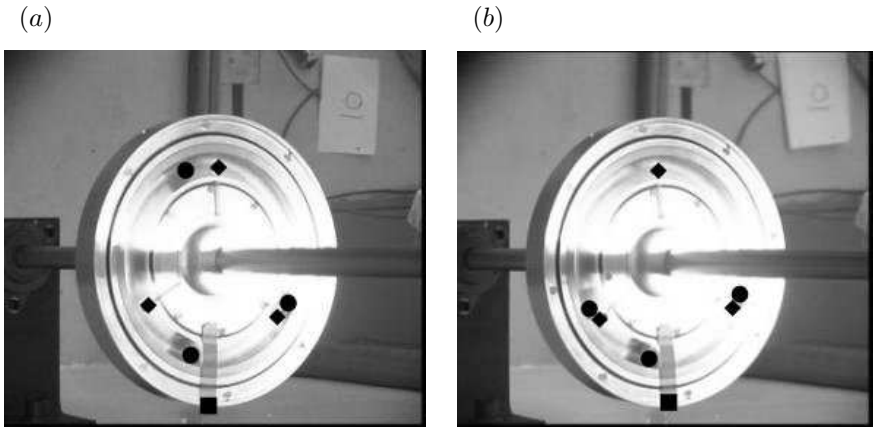

Figure 12. Steady state ball configurations.

(Three-ball steady state configurations (free (a) and coincident (b)). The dots highlight the position of the balls, the diamonds the position of the partitions, and the square the position of the imbalance. Rotation is in the anti-clockwise direction.)

(*b*) *Experimental bifurcation diagrams*

Figure 13 shows, as an example, the vibration spectra obtained for $\omega = 8$ Hz. Specifically, panel (a) shows the vibration spectra for the case in which the balls were fixed, panel (b) shows the vibration spectra for the free ball configuration (figure 12(a)), and panel (c) shows the vibration spectra for the coincident ball configuration (figure 12(b)).

Furthermore, figure 14 shows the overall result of our experimental investigations. The average displacement, taken from the maximum of the first peak of the vibration spectra, averaged over nine runs, is shown versus the rotation frequency. This peak corresponds to the speed of rotation, also known as the 'synchronous response'. The circles correspond to measurements in which the balls were fixed; the squares correspond to measurements in which the balls were free (figure 12(a)); and the crosses correspond to measurements after the free configuration destabilised resulting in the coincident configuration (figure 12(b)).

Quantitative similarities exist between each experimental run. Namely, for the lowest frequencies considered, the free-ball configuration resulted in the least vibration, followed by the coincident and fixed configurations. Increasing the frequency of rotation, interestingly, the free-ball configuration continues to result in a lower vibration than the fixed-ball configuration for a short range of frequencies. However, the fixed-ball configuration is eventually shown to result in the least vibration for higher frequencies. The free-ball configuration is still stable at these higher frequencies, finally becoming unstable at approximately 11.5 Hz ($\Omega = 0.390$). The balls move to the coincident configuration after this instability. As expected, the coincident configuration results in the greatest vibration at all frequencies.

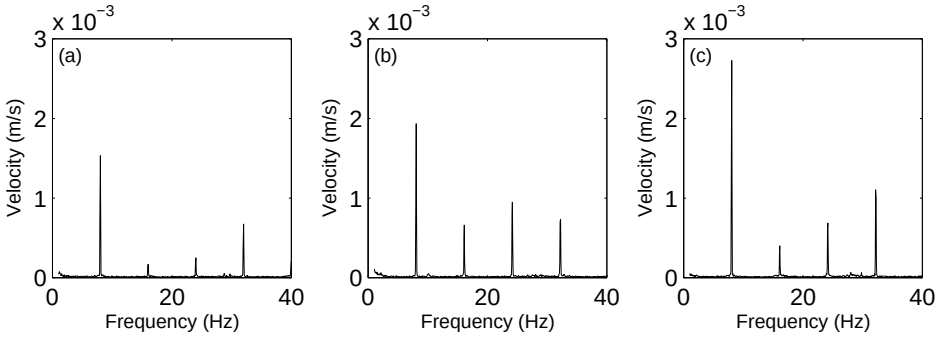

Figure 13. Example of vibration versus speed of rotation for $\omega = 8$ Hz.
(The panels show the vibration spectra for the fixed-ball (a), free ball (b), and coincident (c) configurations.)

6. Numerical bifurcation diagrams

We now compare the experimental results with those obtained using numerical techniques. Namely, we numerically integrate Eqs. (2.9)-(4.1), computing bifurcation diagrams for increasing Ω. Parameters were chosen to correspond to the experiment. Namely, $\delta = 0.0148$, $\mu = 0.011$, $\zeta = 1.4027 \times 10^{-5}$, $r_b = 0.14$, and $e = 0.001$. Furthermore, as β is an uncertain quantity, we perform this analysis for different values of β.

Figures 15(a) to (c) show numerical results computed with `Matlab` for $\beta = 0.1$, 0.3, and 1.0, respectively. Event detection routines where used to model the collisions of the balls with the partitions. After a long initial transient period of $t = 10000$, the extrema of the radial vibration $r = \sqrt{x^2 + y^2}$ have been plotted against the rotation speed Ω. Apart from the initial conditions at $\Omega = 0$ (see below), the initial conditions for each value of Ω were obtained from the immediately preceding value. For a given value of Ω, a single point corresponds to a steady state and a finite number of points corresponds to a periodic vibration. The greater the distance between these points, the greater the amplitude of the oscillation.

In each panel, the *fixed* ball configuration is indicated by circles ($\circ$). Here the balls were fixed at $\phi_1(t) = \pi/3 + r_b$, $\phi_2(t) = \pi + r_b$ and $\phi_3(t) = 4\pi/3 + r_b$, for all $t > 0$. The *coincident* configuration is indicated by crosses ($\times$). Here the initial positions of the balls at $\Omega = 0$ were fixed at $\phi_1(0) = \pi/3 + r_b$, $\phi_2(0) = 4\pi/3 - r_b$ and $\phi_3(0) = 2\pi$. Finally, a *free* ball configuration is indicated by squares ($\square$). Here the initial positions of the balls at $\Omega = 0$ were fixed at $\phi_1(0) = \pi/3 + r_b$, $\phi_2(0) = \pi + r_b$ and $\phi_3(0) = 4\pi/3 + r_b$. After the long transient period of $t = 10000$, the balls are seen to stabilise in a free ball configuration with steady state positions $\phi_1 \approx \pi/3 + r_b$, $\phi_2 \approx \pi + r_b$ and $\phi_3 = 7\pi/3 - r_b$. In other words, the first two balls come to rest a small distance away from their lagging partitions, while the third ball comes to rest against its leading partition. This is slightly different from what was observed experimentally, where the first two balls were shown to stay close to, but move slightly away from, their lagging partitions with the third ball coming to rest at $\phi_3 \approx 2\pi$. We believe that, in the experiment, the balls may be subject to additional

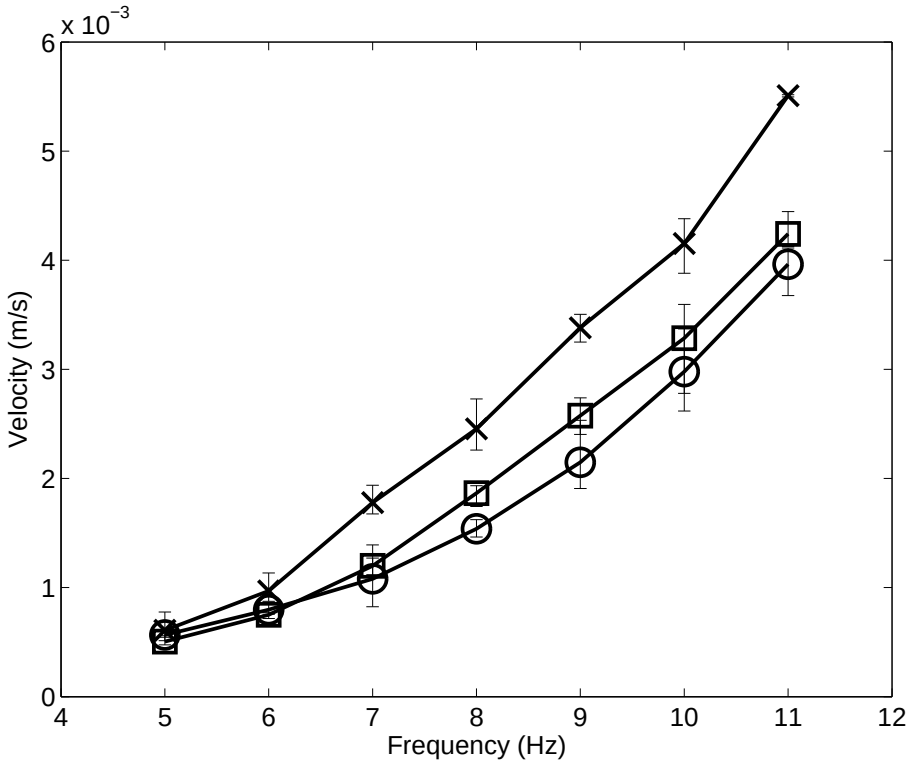

Figure 14. Synchronous response versus speed of rotation.

(Maxima of the first peak of the averaged vibration spectra showing fixed ball positions (circles), free ball positions (squares), and coincident ball positions (crosses). The ends of the error bars correspond to the maximum and minimum deviations from the mean measurements.)

stiction forces (van de Wouw et al. 2005). Such effects are not incorporated in our current model.

After the long transient period, the vibration results shown in each panel are qualitatively the same. The coincident ball configuration (□) is shown to produce the most vibration, followed by the free-ball and fixed-ball configurations, respectively. Both the free-ball and fixed-ball configurations are seen to undergo instabilities (highlighted by a number of points for a given value of Ω) as Ω is increased. Interestingly, this instability is shown to occur at increasingly higher values of Ω as β is increased.

In our experiments, we observed that the free-ball configuration became unstable at a rotation frequency of approximately 11.5 Hz. Given that the resonant frequency was measured to be 29.5 Hz, this corresponds to an instability at $\Omega \approx 0.39$. Thus suggesting that the internal damping in our experiments corresponds to a value of β of order one. Furthermore, in experiments, after this instability the balls moved to the coincident-ball configuration. This is not observed in our numerical investigations. Instead, the free-ball configuration is shown to destabilise to more

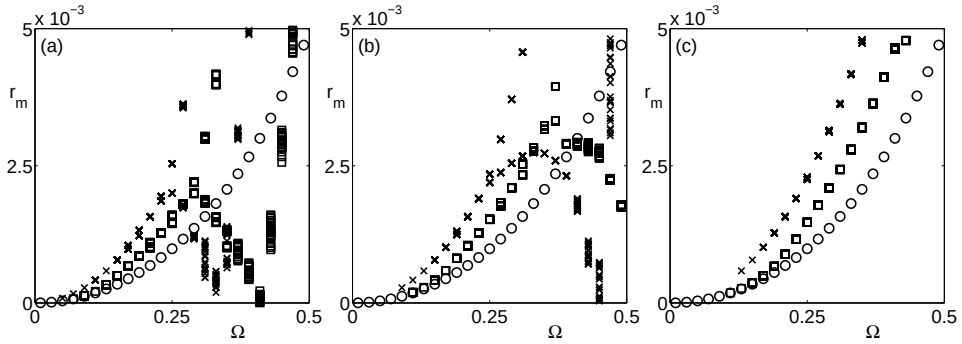

Figure 15. Numerical bifurcation diagrams showing extrema of the radial displacement versus rotation speed.

(Bifurcation diagrams obtained by numerical integration, showing the extrema r_m of the radial vibration $r = \sqrt{x^2 + y^2}$ against rotation speed Ω. Parameters were fixed at $\zeta = 1.4027 \times 10^{-5}$, $\delta = 0.0148$, and $\mu = 0.011$; and from (a) to (c), $\beta = 0.1$, 0.3 and 1.0, respectively. Circles correspond to the fixed-ball configuration, squares to a free-ball configuration, and crosses to the coincident-ball configuration. Note that $\Omega \in [0, 0.5]$ corresponds to a physical rotor speed of $\omega \in [0, 14.75]$ Hz.)

complex dynamics which still do not reach the level of vibration of the coincident ball configuration. Specifically, these dynamics correspond to each ball repeatedly impacting its front and back facing partitions.

7. Conclusions

The aim of the this paper has been to take the earlier bifurcation studies of Chung & Ro (1999), Adolfson (2001) and Green et al. (2006a) and draw practical conclusions. To this end, we have designed and built an experimental rig. This rig is capable of assessing the suitability of automatic dynamic balancers at improving the vibration characteristics of eccentric rotors that are below their fundamental resonance frequency. The experiments repeatedly identified two steady state configurations of the balls. One configuration was shown to add as much mass as was possible, subject to the partition constraints, to the imbalance. This configuration was analogous to the coincident steady state of the ADB without the partitions. The second configuration corresponded to all balls coming to rest away from a partition. This was shown to slightly add to the imbalance for the majority of rotation speeds. However, measurements repeatedly showed a reduction in the imbalance, and a lower radial vibration than for a fixed-ball configuration, for the lowest rotation speeds investigated. Bifurcation diagrams obtained by numerical integration of the equations of motion describing this impacting system revealed similar results. In particular, numerical simulation confirmed the existence of a free-ball configuration, similar to the one identified in the experiments. We believe that the discrepancies between our numerical and experimental results are due to stiction forces, which are not currently incorporated into our model.

The simplest conclusion from these results is that, despite the existence of various equilibrium positions of the balls which in theory could improve the eccentric

vibrations, the ADB does not help for such rotation speeds. While this conclusion may appear somewhat negative, there are several important steps we have established in understanding the consequences of the nonlinear dynamical analysis on the design of ADBs.

First, we have investigated the effects of using more than two balls. The results are mixed. Increasing the number of balls, increases the number of possible equilibrium states and also the number of internal degrees of freedom within the perfectly balanced state. Intuitively these extra equilibria may give rise to more robustness and larger basins of attraction of the balanced state, and we have found some evidence to support this. However, increasing the number of balls appears to decrease the range of parameter values at which balance is possible. Further detailed comparison would be necessary for a particular rotor geometry and operating rotation speeds to ascertain how many balls would be optimal.

Second, we have established the advantages of the use of partitioned ball races, with one ball in each partition. This simple modification to the simplest design obviates the need for complex release mechanisms that clamp the balls to the rotor until a desired rotation speed is reached.

Third, we have established partial agreement between our experimental results and simulations of the numerical model. Note that bifurcation studies of the problem containing partitions are not straightforward, due to the presence of non-smooth impacting behaviour. Future work may use recently developed bifurcation software for impacting systems which will allow the detection of non-smooth bifurcations (Budd et al. 2005) in addition to steady-state and Hopf bifurcations that occur in the smooth system.

It has been beyond the scope of this paper to investigate all possible nonlinear dynamics of the ADB with more than two balls, either with or without partitions. Green et al. (2006a, 2006b) have shown the necessity of these studies in understanding the actual behaviour of the system, including transient effects and multi-stability between competing stable states. These studies are likely to be especially important for super-critical rotors (for which $\Omega > 1$) which we have shown are likely to be the only kinds of system for which an ADB might be effective. The building of a lightweight, low bearing stiffness, experimental rig would appear to be pressing, since our current experimental set-up is not able to access such rotation speeds.

Another important issue worthy of further study is to look at the combined effects of viscous damping, stiction and impacts with partitions in the ball race. It is likely that stiction could in fact be playing a role in the experiments described in this paper, resulting in some of the differences with the numerical simulations. Other geometries are also possible for the implementation of the balancing masses, e.g., pendula or paddles mounted at separate axial positions on the shaft (Horvath & Flowers 2005). It is clear from the bifurcation studies that ball race damping is one of the key parameters governing the existence and robustness of the stable balanced state and more modelling effort needs to put into to characterising how this damping arises in practice.

Finally, we have only looked at the use of ADBs to balance eccentric rotors. Work in progress is looking at using multiple ADB disks which might also correct for vibrations due to couple imbalance.

The authors would like to thank Jorge Galán Vioque for helpful discussions, Clive Rendall and Tony Griffith for continued technical support while designing, building and running

the experimental rig, and Marian Wiercigroch for his comments on an earlier draft. KG was funded by the EPSRC grant GR/535684/01. MIF gratefully acknowledges the support of the Royal Society through a Royal Society-Wolfson Research Merit Award. The visit of AMM to Bristol was made possible through the EU Socrates/Erasmus scheme.

References

Adolfsson, J. 2001. Passive Control of Mechanical Systems: Bipedal Walking and Autobalancing. Ph.D. thesis, Royal Institute of Technology, Stockholm.

Budd, C., di Bernardo, M., Champneys, A. R., Nordmark, A. B., Olivar, G., & Piiroinen, P. T. 2005. Bifurcations in Nonsmooth Systems. BCANM Technical Report. `http://www.enm.bris.ac.uk/anm/preprints/2005r04.html`

Chung, J. & Ro, D. S. 1999. Dynamic analysis of an automatic dynamic balancer for rotating mechanisms. *Journal of Sound and Vibration* **228**, 1035–1056.

Dhooge, A., Govaerts, W., Kuznetsov, Y. A., Mestrom, W., and Riet, A. M. 2004. MATCONT: A continuation toolbox in Matlab.

Ernst, H. 1951. Automatic precision balancing. *Machine Design*.

Green, K. 2005. Analysis of an automatic dynamic balancing mechanism for eccentric rotors. In van Campen, D. H., Lazurko, M. D. & van den Oever, W. P. J. M. (eds.) 2005. *Fifth EUROMECH Nonlinear Dynamics Conference*, ISBN 90 386 2667 3.

Green, K., Champneys, A. R., & Lieven N. J. 2006a. Bifurcation analysis of an automatic dynamic balancing mechanism for eccentric rotors. *Journal of Sound and Vibration* **291**, 861–881.

Green, K., Champneys, A. R., & Friswell M. I. 2006b. Analysis of the transient response of an automatic dynamic balancer for eccentric rotors. *International Journal of Mechanical Sciences* **48**, 274–293.

Horvath, R. & Flowers, G. T. 2005. Passive balancing for rotor systems using pendulum balancers. *Proceedings of the 20th ASME International Biennial Conference on Mechanical Vibration and Noise*.

Huang, W.-Y., Chao, C.-P., Kang, J.-R., & Sung, C.-K. 2002. The application of ball-type balancers for radial vibration reduction of high-speed optic drives. *Journal of Sound and Vibration* **250**, 415–430.

Hwang, C.-H. & Chung, J. 1999. Dynamic analysis of an automatic ball balancer with double races. *JSME International Journal: Series C* **42**, 265–272.

Jeffcott, H. H. 1919. The lateral vibration of loaded shafts in the neighbourhood of a whirling speed – the effect of want of balance. *Philosophical Magazine Series 6* **6**, 304–314.

Kim, W. & Chung, J. 2002. Performance of automatic ball balancers on optical disc drives. *Proc Instn Mech Engrs Part C: J Mechanical Engineering Science* **216**, 1071–1080.

Kuznetsov, Yu. A. 1997. *Elements of Applied Bifurcation Theory*, Springer, Berlin.

Lee, J. & Van Moorhem, W. K. 1996. Analytical and experimental analysis of a self-compensating dynamic balancer in a rotating mechanism. *ASME Journal of Dynamic Systems, Measurement and Control* **118**, 468–475.

Majewski, T. 1987. Synchronous vibration eliminator for an object having one degree of freedom. *Journal of Sound and Vibration* **112**, 401–413.

Rajalingham, R. & Rakheja, S. 1998. Whirl suppression in hand-held power tool rotors using guided rolling balancers. *Journal of Sound and Vibration* **217**, 453–466.

Sharp, R. S. 1975. An analysis of a self-balancing system for rigid rotors. *J. Mech. Engng. Sci.* **17**, 186–189.

Thearle, E. 1932. A new type of dynamic-balancing machine. *Transactions of ASME* **54**, 131–141.

van de Wouw, N., van den Heuvel, M. N., van Rooij, J. A. & Nijmeijer, H. 2005. Performance of an automatic ball balancer with dry friction. *Int. J. Bifurcation and Chaos* **15**, 65–82.